

## Article

# Synthesis and Performance Evaluation of a Novel High-Temperature-Resistant Thickener

Yu Sui <sup>1,2</sup>, Tianyue Guo <sup>1,2,\*</sup>, Dan Li <sup>1</sup>, Da Guo <sup>3</sup>, Zhiqiu Zhang <sup>1</sup> and Guangsheng Cao <sup>1,\*</sup>

<sup>1</sup> Key Laboratory of Enhanced Oil Recovery, Ministry of Education, College of Petroleum Engineering, Northeast Petroleum University, Daqing 163318, China; n2107778k@e.ntu.edu.sg (Y.S.); ldnepu0520@163.com (D.L.); zhang\_zhiqiu@126.com (Z.Z.)

<sup>2</sup> School of Mechanical and Aerospace Engineering, Nanyang Technological University, 50 Nanyang Avenue, Singapore 639798, Singapore

<sup>3</sup> China Petroleum Tarim Oilfield Branch Oil and Gas Engineering Research Institute, No. 26, Shihua Avenue, Korla 841001, China; 18646660514@163.com

\* Correspondence: n2107777b@e.ntu.edu.sg (T.G.); caoguangsheng@nepu.edu.cn (G.C.)

**Abstract:** Successful exploitation of carbonate reservoirs relies on the acid-fracturing process, while the thickeners used in this process play a key role. It is a common engineering problem that thickeners usually fail to function when used in high-temperature environments. Until now, no research has ventured into the field of synthesizing thickeners which can be effectively used at ultra-high temperatures up to 180 °C. In our current study, a novel high-temperature-resistant polyacrylamide thickener named SYGT has been developed. The thermal gravimetric analysis (TGA) reveals that SYGT is capable of withstanding temperatures of up to 300 °C. Both our scanning electron microscopy (SEM) and rheological analysis demonstrate that the SYGT exhibits excellent resistance to both temperature and shear. At 180 °C, the viscosity of the SYGT aqueous solution is no lower than 61.7 mPa·s at a 20% H<sup>+</sup> concentration or high salt concentration, and the fracture conductivity of the thickened acid reaches 6 D·cm. For the first time, the influence of the polymer spatial network's structural parameters on the viscosity of polymer solutions has been evaluated quantitatively. It was discovered that the length and surrounding area of the SNS skeleton have a synergistic effect on the viscosity of the polymer solution. Our experiments show that SYGT effectively reduces the acid–rock reaction rate and filtration loss under harsh working conditions such as high temperature, strong shear, high salinity, and a high concentration of acid. The synthesized acid-fracturing thickener (SYGT) has wide application potential in the development of carbonate reservoirs under high-temperature conditions.

**Keywords:** carbonate reservoir; temperature stability; polyacrylamide; spatial network structure



**Citation:** Sui, Y.; Guo, T.; Li, D.; Guo, D.; Zhang, Z.; Cao, G. Synthesis and Performance Evaluation of a Novel High-Temperature-Resistant Thickener. *Molecules* **2023**, *28*, 7036. <https://doi.org/10.3390/molecules28207036>

Academic Editors: Katsuhiko Ariga, Fabien Grasset and Yann Molard

Received: 14 September 2023

Revised: 2 October 2023

Accepted: 2 October 2023

Published: 11 October 2023



**Copyright:** © 2023 by the authors. Licensee MDPI, Basel, Switzerland. This article is an open access article distributed under the terms and conditions of the Creative Commons Attribution (CC BY) license (<https://creativecommons.org/licenses/by/4.0/>).

## 1. Introduction

Carbonate reservoirs hold 60% and 40% of the world's total oil and gas reserves, respectively. To ensure their efficient development is vital for global energy security [1,2]. Acidizing fracturing, which constructs highly conductive fractures, can greatly boost oil and gas production [3–6]. The effectiveness of acidizing fracturing is evaluated by the effective action distance of acid and the conductivity of acid etch fracture [7–11]. However, conventional acidizing fracturing is hindered by the rapid reaction between hydrochloric acid and carbonate minerals, which results in significant wastage of hydrochloric acid in the near-well zone, while the far-well zone experiences poor acidizing fracturing effects [12]. A slow-release acid system has been developed to address this challenge by reducing the mass transfer coefficient of H<sup>+</sup> and the acid–rock reaction rate by increasing the viscosity of the acid solution or chemically generating acid. This procedure can increase the effective acid action distance and allow the acid to penetrate deeper into the formation [13]. Gelled acid is a form of slow-release acid that exhibits good sand carrying, drag reduction, and

filtration loss reduction properties [14–18]. Consequently, gelled acid is widely employed in the acid fracturing of carbonate rock.

The efficacy of thickened acid is dependent on the type of thickener used [19]. Thickeners are categorized as biological, cellulose, and synthetic polymers [20]. Biological polymers are unstable in high acid concentrations, and possess low temperature resistance, which limits their applicability [21,22]. Similarly, cellulosic-based polymers degrade easily, have poor shear resistance, and exhibit low temperature resistance, which make them unsuitable for use in oil fields [23]. Presently, the most widely used thickener is synthetic polyacrylamide [24,25]. However, with the increasing use of acidizing fracturing in high temperatures and deep wells in carbonate reservoirs, the amide group in polyacrylamide undergoes chemical degradation, causing molecular chains to shear, reducing molecular weight and hydrodynamic volume, and resulting in a decrease in viscosity, as seen in Figure 1a. Therefore, the viscosity of the thickened acid is significantly reduced under high-temperature conditions, resulting in a short effective acid action distance, a low conductivity of the acid-etched fracture, and a poor acid-fracturing effect. In this context, polyacrylamide's temperature resistance poses new challenges. Additionally, as freshwater resources are scarce, using high-salinity brine or seawater directly to prepare acidifying fluids for fracturing has become a trend [26]. In deep formations, fluids typically have high salinity, which demands higher salt resistance from the acid solution. In addition, the adsorption of polyacrylamide in carbonate reservoirs also leads to a decrease in the concentration of effective components in the fracturing fluid, resulting in a decrease in viscosity [27,28].

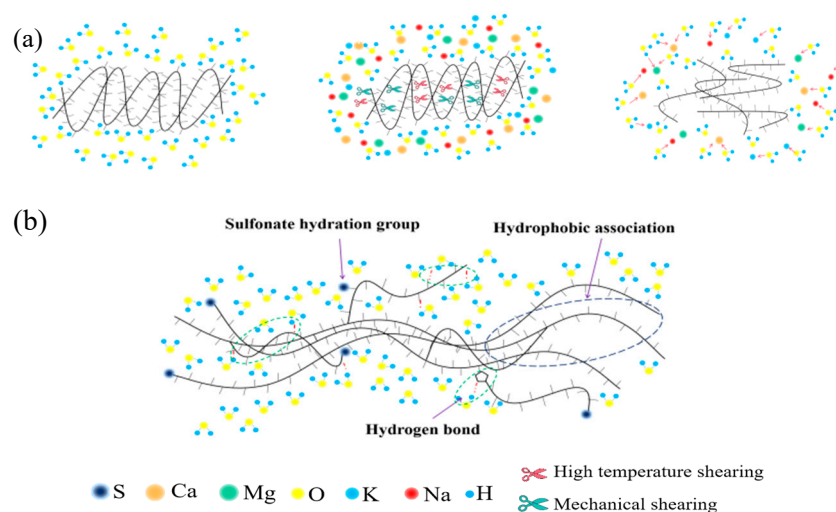


**Figure 1.** (a) Failure principle of thickener under high temperature, high salt and strong shear; (b) Schematic diagram of partial mechanism of temperature and salt resistance of synthetic SYGT.

In recent years, numerous studies have been conducted to improve the temperature and salt resistance of polyacrylamide [29–32]. Various strategies have been employed to enhance the temperature resistance of polyacrylamide, including the incorporation of rigid groups into the polyacrylamide backbone [33–36], such as sulfonic acid groups and cyclic materials, as reported in previous studies. Recently, a double quaternary ammonium salt copolymer has been synthesized [37], which exhibits remarkable temperature resistance and maintains a viscosity of 67 mPa·s at 170 °C. The results suggest that the incorporation of such groups into polyacrylamide molecules could improve their high-temperature stability, rendering them suitable for enhanced oil recovery (EOR) applications in harsh reservoir conditions. Despite the promising results obtained in those studies, further investigations are required to improve the experimental temperature and evaluate the viscosity of the system at an ultra-high ambient temperature, such as 180 °C, which has not yet been explored. Furthermore, research on the salt resistance of the system is limited. The high salinity, espe-

cially in the presence of divalent cations [38], has a significant impact on the electrostatic shielding effect [39], resulting in the entanglement of polymer molecules and weakening the viscosity-increasing effect. Moreover, the cations carried by polymers can disrupt the formation of worm-like micelles in the formation of water with high salinity, leading to a loss of viscoelasticity [40]. In this regard, some researchers have focused on improving the performance of crosslinking agents to enhance the stability of polymers. For instance, a covalent bond between polyethyleneimine and amide in NFT [41] can form crosslinking, which has been shown to impart superior temperature resistance to the resulting polymer solution. The development of various cross-linking agents to enhance polymer stability has been carried out, and the effectiveness of the developed agents has been verified. However, operational costs are also increased accordingly. Other researchers have focused on developing the polymer itself, such as hydrophobically associating polyacrylamide (HAPAM). They use acrylamide, acrylic acid, etc. as the main body, then modify them by introducing hydrophobic monomers to improve the linear flexible chain to a certain extent. A cationic hydrophobically associative polymer polyacrylamide [42] (C-HAPAM) has demonstrated good temperature and salt resistance under experimental conditions. The hydrophobic part incorporated into the main polymer chain is bonded in the water phase through intramolecular and intermolecular interactions to enhance the stability of the molecule. However, the experimental temperature of this study is relatively low, at 105 °C only. From the above discussion, it is apparent that there is a lack of research on developing a high-temperature-resistant polyacrylamide acid thickener. While there are several synthetic thickeners available for fracturing fluid, most polyacrylamide-based thickeners have poor acid resistance that has not been adequately investigated. This underscores the pressing need for a thickener that can withstand high temperatures and minimize viscosity loss when used in acidic fluids to address the current challenges associated with the thickening and acid fracturing of carbonate rocks.

In our current research, we have synthesized quaternary ammonium polymers based on AM (acrylamide), AMPS (2-acrylamido-2-methylpropanesulfonic acid), NVP (N-vinyl-2-pyrrolidone), and SSS (sodium polystyrene sulfonate). Additionally, we have synthesized ternary polymers using AM, AMPS, and SSS as starting materials for comparison purposes. The structures of the obtained polymers have been confirmed by infrared spectroscopy. The temperature and salt resistance mechanism of the copolymer are shown in Figure 1b. The rheological properties, temperature, salt resistance, and shear resistance of the polymer are evaluated through thermogravimetric analysis using rheometers and Brinell viscometers. The action mechanism of the spatial network structure (SNS) on the viscosity of the polymer solution is analyzed through SEM pictures and AutoCAD. The obtained viscosity of the polymer under acidic conditions is compared, and the mechanism of H<sup>+</sup> action on the polymer is analyzed. Finally, the thixotropy, reaction kinetics, and filtration of the thickened acid system have been evaluated. The effect of the thickened acid is analyzed through experiments. Our investigation aims to propose a new type of high-temperature-resistant thickened acid-fracturing thickener, and explore the specific action mechanism of SNS on the viscosity of polymer solutions.

## 2. Results and Discussion

### 2.1. Synthesis and Characterization of SYGT

To design functional polymers, corresponding polymer synthesis experiments were carried out with acrylamide as the main chain, and monomers with rigid chain structures that exhibit high temperature and acid resistance as the side chain. The focus was not on maximizing yield but on achieving desirable properties. The formation of jelly-like gel indicates that the polymerization between the reaction monomers is successful, and a polymer with a viscosity-increasing effect is formed. With the progress of the reaction, the viscosity of the produced system gradually increases. The synthetic pathway is shown in Figure 2.

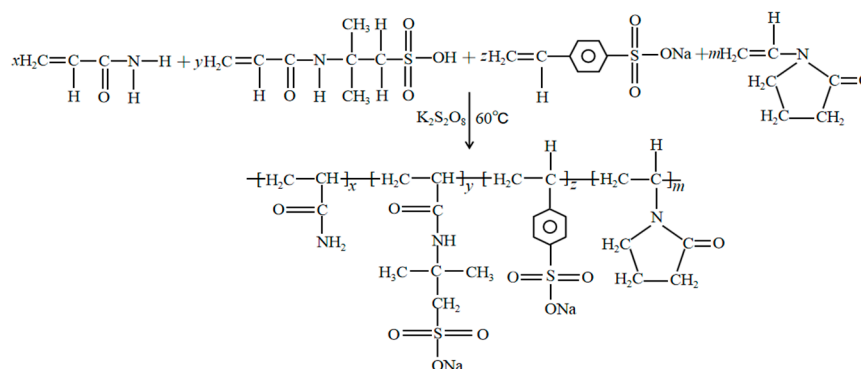


**Figure 2.** Schematic diagram of synthesis principle.

After squeezing the solid powder with a press, infrared mapping scanning was conducted using a Spectrum One FT-IR Spectrometer to verify the synthetic results of AM/AMPS/SSS polymer and AM/AMPS/NVP/SSS polymers, as depicted in Figures 3a and 3b, respectively.

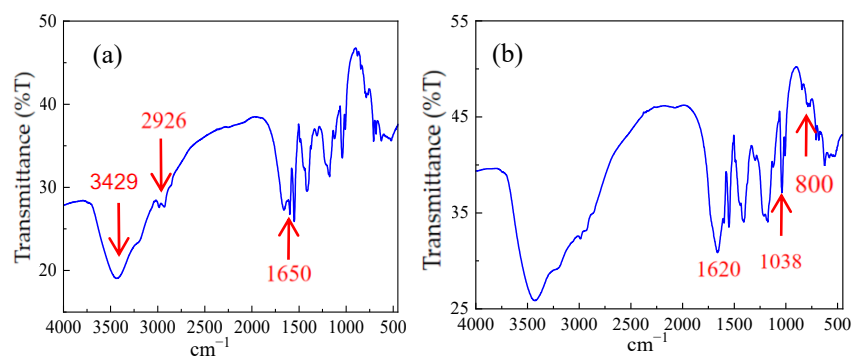


**Figure 3.** (a) Infrared spectrogram of ternary polymer; (b) Infrared spectrogram of quaternary polymer.

Generally speaking,  $3429\text{ cm}^{-1}$  is the characteristic absorption peak of free  $-NH_2$ ,  $3216\text{ cm}^{-1}$  is the characteristic absorption peak of associated  $-NH_2$ ,  $2926\text{ cm}^{-1}$  is the characteristic absorption peak of the methylene antisymmetric stretching vibration, and  $2850\text{ cm}^{-1}$  is the characteristic absorption peak of the methylene symmetric stretching vibration. The infrared spectra reveal that the characteristic peak of amide II (N–H bending vibration) is located at  $1620\text{ cm}^{-1}$ , the strong absorption peak around  $1650\text{ cm}^{-1}$  is attributed to the amide group, and the absorption peak at  $1038\text{ cm}^{-1}$  is associated with the sulfonic acid groups. Furthermore, the characteristic absorption peak of the p-disubstituted benzene appears at  $800\text{ cm}^{-1}$ . A significant increase in peak intensity at  $1561\text{ cm}^{-1}$ , corresponding to the secondary amide N–H bending vibration, was observed after cationization, indicating that N–H in polyacrylamide was replaced by N–R. Additionally, the peak at  $1174\text{ cm}^{-1}$  is common in cationized products; it is generally related to C–N, and confirms that both the ternary and quaternary polymers synthesized are cationic polymers.

## 2.2. TGA Results and Analysis

The decomposition temperature of polymers mainly depends on the thermal stability of macromolecular groups. The introduction of the sulfonic acid group and benzene rings leads to an increase in the molecular weight of SYGT, and greatly enhances the temperature resistance of SYGT. The TGA (thermogravimetric analysis) and DTG (differential thermogravimetric analysis) curves of SYGT are shown in Figure 4.

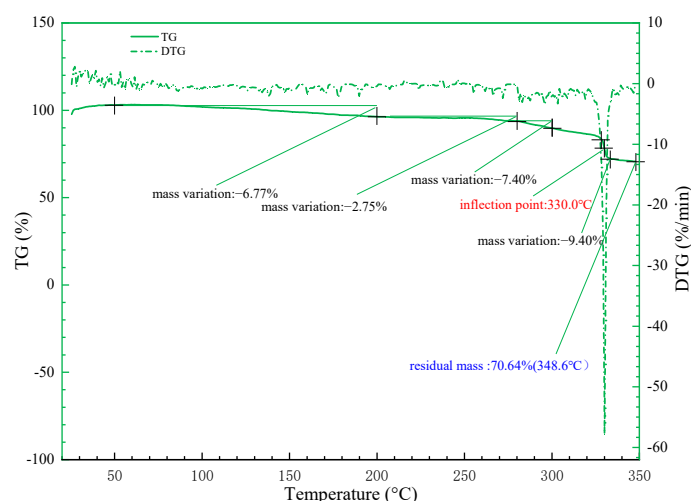


**Figure 4.** SYGT thermogravimetric curve.

Thermogravimetric analysis was conducted to evaluate the thermal stability of the polymer in the temperature range of 25–350 °C. The polymer exhibited relatively stable thermal decomposition at the experimental temperature, with a noticeable decline in mass occurring at 330 °C.

There was no obvious mass loss of the polymer at 25–100 °C, indicating that the sulfonic acid and acrylamide groups in the polymer had already removed the adsorbed water in the drying chamber. At 280–320 °C, the polymer mass decreased relatively significant, at 7.4%. The most significant mass loss of 9.4% occurred near 330 °C. The DTG curve indicated that the change was the largest at this temperature, and the final (348.6 °C) mass residual rate was 70.64%. In order to verify the thermal stability of the polymer, the study results of Zhang [43] are compared with the current thermal stability of SYGT. At about 350 °C, the polymer weight loss rate studied by Zhang is generally lower than 70%, around 60%. A comparative analysis of the thermal stability data proves that SYGT has better thermal stability.

### 2.3. Rheological and Temperature Resistance Test

The rheological properties of ternary polymers and SYGT at 120, 135, 150, 165 and 180 °C are shown in Figures 5a and 5b, respectively. The corresponding viscosity loss rates at different temperatures are shown in Figure 5c.

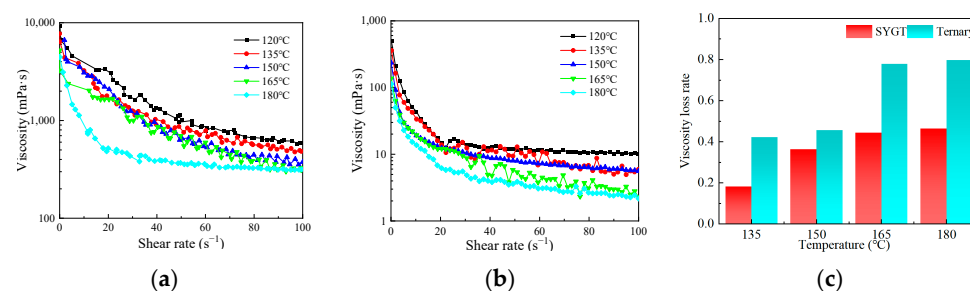


**Figure 5.** (a) Rheology of SYGT; (b) Rheology of ternary polymers; (c) Viscosity loss rate at different temperatures.

It can be seen from Figure 5a,b that both the rheology of terpolymer and SYGT decrease as the temperature and shear rate increase. The molecular chain of polyacrylamide is broken with increasing temperature, resulting in shorter molecular chains and the destruction of the spatial network structure of the polymer. The molecular hydrodynamic volume becomes smaller, and the viscosity of the polymer solution decreases macroscopically. Similarly, as the shear rate increases, the mechanical shear effect becomes more pronounced, resulting

in a shorter molecular weight and a decrease in the polymer viscosity. In comparison to the viscosity of the existing thickeners at 180 °C, which is approximately 50 mPa·s, SYGT exhibited a viscosity of 316 mPa·s, and demonstrated remarkable viscosity-increasing and temperature resistance properties.

The viscosity of SYGT at 180 °C decreased by 46.45%, while the terpolymer showed a greater decrease of 79.82% compared to that at 120 °C, as depicted in Figure 5c. It should be noted that the viscosity average molecular weight of the synthesized ternary polymer is  $8.23 \times 10^5$ , and the molecular weight of SYGT is  $8.57 \times 10^5$ . The difference in molecular weight between the two is not significant, although SYGT is a quaternary copolymer. This result indicates that SYGT has superior temperature resistance compared to the terpolymer. In addition, the viscosities of SYGT and the terpolymer are significantly different. Under a shear rate of 180 °C and  $100 \text{ s}^{-1}$ , the viscosity of SYGT remained 316.52 mPa·s, indicating a remarkable viscosity-increasing effect.

To explore the temperature resistance mechanism of the polymer, its morphology was studied using scanning electron microscopy for the polymer solutions at temperatures of 20 °C, 120 °C, 135 °C, 150 °C, 165 °C, and 180 °C, respectively, as shown in Figure 6.

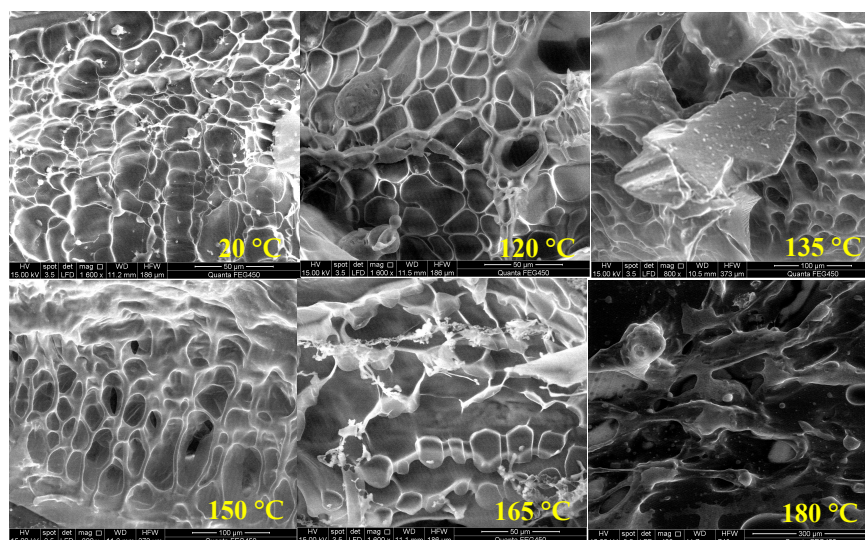


**Figure 6.** Polymer morphology at different temperatures.

At 20 °C, a distinctive “fish-scale” spatial network structure (SNS) is visible in the polymer solution under SEM. With increasing temperature, the SNS is progressively disrupted. The local “fish scales” are fractured and no longer appear as a cohesive structure, particularly at 165 °C and 180 °C. The hydration structure formed by the polymer molecules is destroyed, and the hydrodynamic volume is reduced.

In order to explore the shear resistance of SYGT at high temperatures, a shear test was performed at  $170 \text{ s}^{-1}$  and 180 °C for 160 min, respectively. The experimental results show that the viscosity loss rate is 54.01%, and the viscosity is 145.95 mPa·s. It can be seen from the data that SYGT has competent shear resistance under high-temperature conditions, as shown in Figure 7.

As the shear time increases, the viscosity gradually decreases and tends to reach a stable state, indicating that the establishment and destruction of the polymer’s spatial network structure have reached a balance, which is proven in Figure 8. After shearing the polymer for 60 min, compared with the case of 20 min shearing, the degree of SNS damage is greater. After 120 min of shearing, the damage degree is slightly increased compared with the case of 60 min of shearing, but the SNS is basically stable.

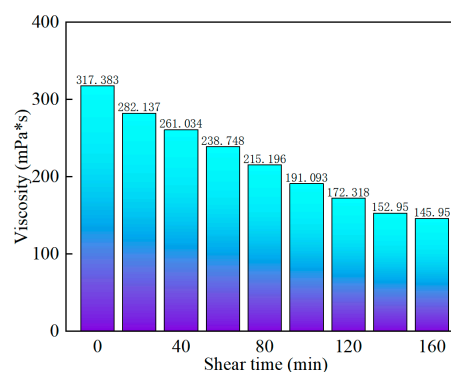


**Figure 7.** Variation in polymer viscosity with shear time.

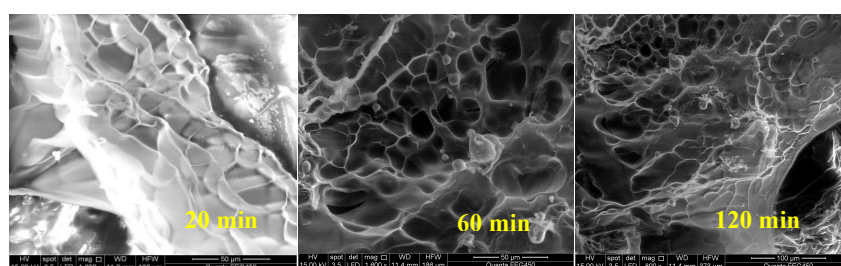


**Figure 8.** Morphology of polymer solution after shearing at different time.

#### 2.4. Effect Mechanism of SNS on Viscosity

Based on our current research, it is concluded that temperature affects the size of polymer molecules through the “high-temperature shear” of polymer chain, leading to changes in the spatial network structure of polymer aqueous solutions and ultimately affecting the viscosity of the solution. However, the impact of specific parameters related to the distribution of the polymer’s spatial network structure on the solution’s viscosity remains understudied. Just like the trunk and branches of a tree, the density and thickness will affect the distribution of leaves, and the leaves will affect the flow of air. The distribution width of the polymer solution space network framework is also fundamental to the formation of a polymer control body by the polymer-constrained water molecules. However, the distribution and skeleton width of the polymer molecules under different temperatures, concentrations, and shear conditions of a shear body are different, thus showing different levels of aqueous solution viscosity.

The SEM image presented in Figure 6 is processed using AutoCAD 2023 software to obtain the skeleton line of the SNS, as shown in Figure 9a.

The length and surrounding area of the SNS skeleton are calculated using AutoCAD. The magnification of the picture is inconsistent during processing, but the statistical results of AutoCAD, including the length and area, are made to be dimensionless, which eliminates the impact of inconsistent magnification. The statistical results are shown in Figure 9b.

It is seen from Figure 9b that the skeleton length of SNS decreases with increasing temperature, and its value at 180 °C is only 17.27% of that at 120 °C. The polymer molecular chain is continuously sheared with increasing temperature. The control ability of the fluid is continuously reduced, which leads to continuous reduction in the skeleton length of the airborne network structure. The overall distribution also continuously becomes sparse. From a two-dimensional perspective, the utilization of the plane is reduced, as shown in Figure 9a.

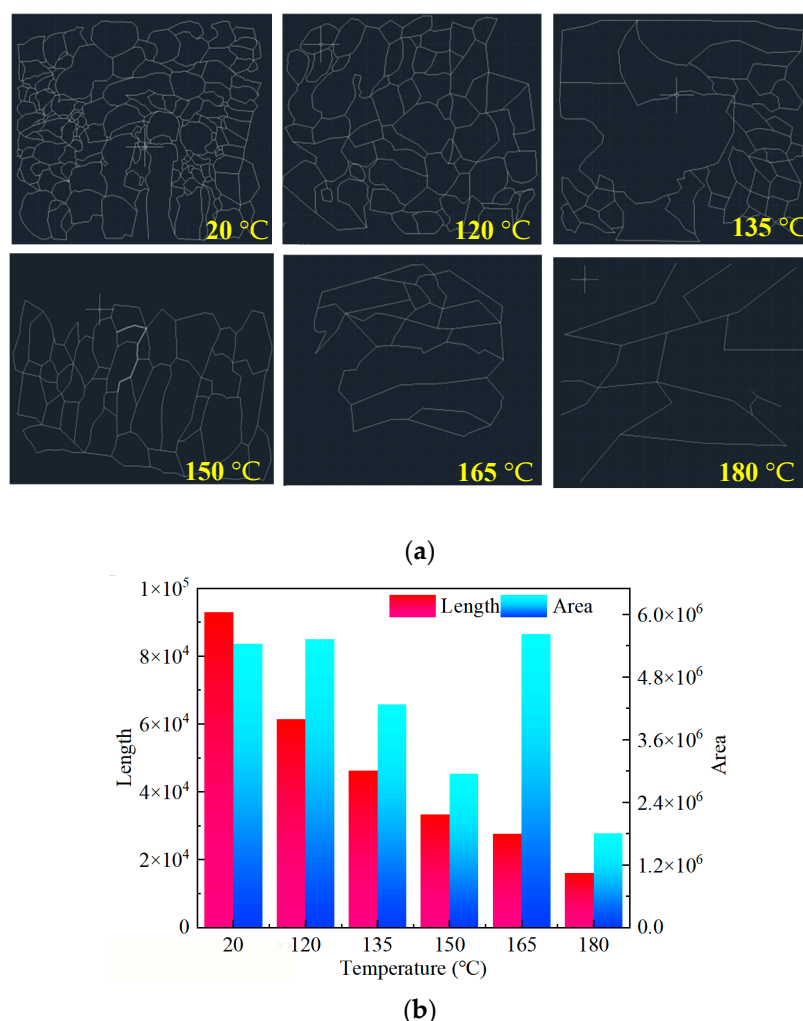


**Figure 9.** (a) SEM image of the SNS skeleton; (b) Length and area statistics of the SNS skeleton.

The area surrounding the skeleton also shows a negative correlation with the increase in temperature. However, there was a certain increase at 165 °C. The drawn SNS skeleton is basically composed of closed lines. Although the enclosing area is large at 165 °C, as can be seen from Figure 6, the actual fluid control in the area of the polymer is not the same as in its enclosing area. Therefore, the enclosing area at 165 °C is overestimated in the calculation process. This also indicates the existence of a certain synergistic effect between the length and enclosing area of the SNS. Even if the SNS area is large enough, it still requires a long enough skeleton to support it, and a reasonable spatial layout is needed; otherwise, it is difficult to form a continuous and effective water molecule control body.

From the above analysis, it is evident that the length and surrounding area of the SNS skeleton have a synergistic effect on the viscosity of the polymer solution. Therefore, in future research, it will be necessary to refine the influence of the SNS skeleton parameters on the viscosity of the polymer solution. This includes expanding the parameters, quantifying their effects, and ultimately deriving a consensus on the relationship between the SNS skeleton and the viscosity of the polymer solution.

### 2.5. Acid and Salt Resistance Test

The acid concentration used on the field is typically 20%, but with the reaction between acid and rock, the acid concentration gradually decreases. To investigate the effect of acid concentration on the viscosity of SYGT solution, 1 g of the SYGT was dissolved in 100 mL acid solution with varying concentrations. The upper limit of acid solution concentration is set at 20%. The viscosity was measured at 180 °C with a shear rate of 170 s<sup>-1</sup>. The results

showed that the viscosity of SYGT solution decreased with the increasing acid concentration, and then leveled off. At an acid concentration of 20% HCl, the solution viscosity of SYGT was 61.7 mPa·s, as shown in Figure 10a. Hydrogen ions induce the crimping of the molecular chains of SYGT, leading to an improvement in hydrogen bond interaction (within the molecules) and a reduction in the hydrodynamic radius. Additionally, the oxidation of  $H^+$  attracts the electrons in the shared electron pair, thereby affecting the stability of the shared electron pair. From Figure 10c, the spatial structure was significantly damaged, changing from mesh to rod, resulting in a decrease in the polymer viscosity.

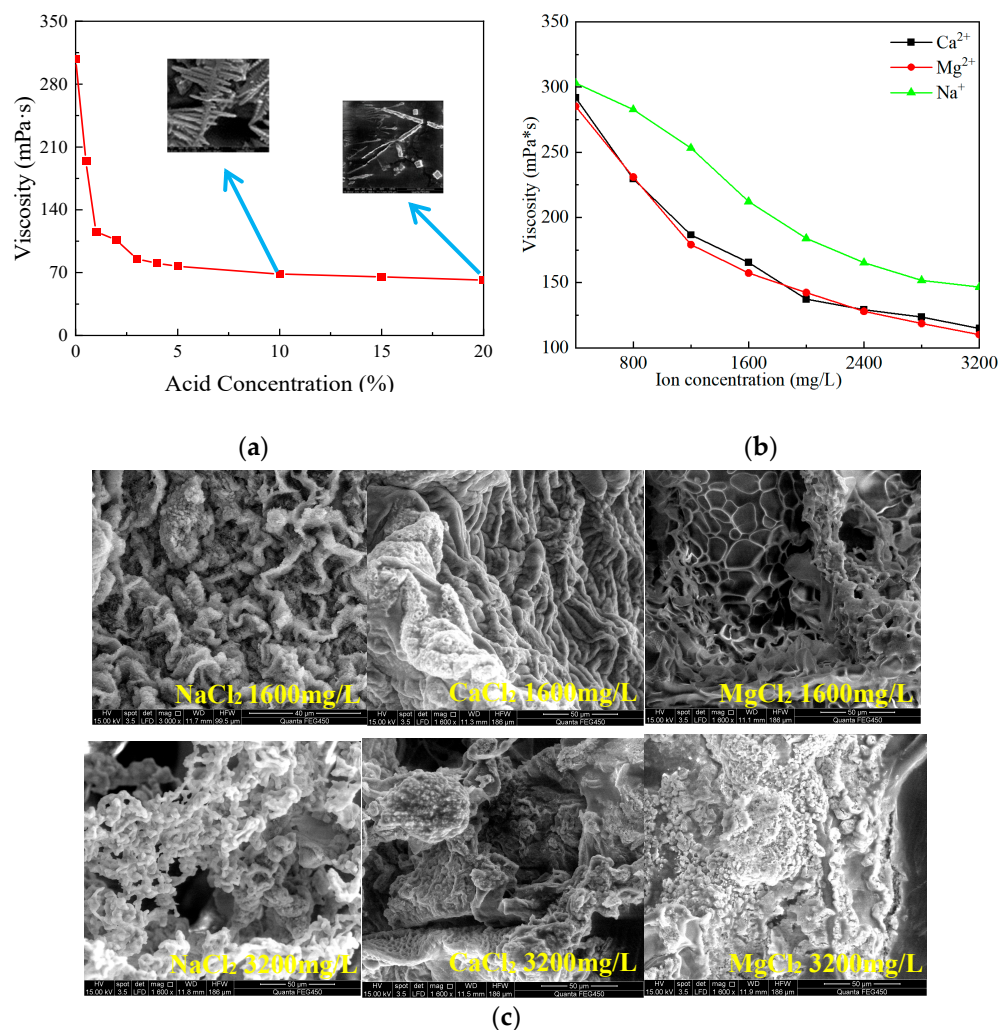


**Figure 10.** (a) Variation in viscosity with acid concentration; (b) Viscosity versus inorganic salt concentration; (c) SEM images of SYGT under different conditions.

As mentioned in the introduction, due to a shortage of fresh water resources, it has become a trend to prepare acid solutions with seawater. To evaluate the salt resistance of SYGT, the salinity (0.32 g/L) of the seawater in Liaodong Bay of Bohai Sea [44] was taken as the upper limit.

The viscosity of the SYGT solution gradually decreased and finally stabilized with the increasing inorganic salt ion concentration, as seen in Figure 10b. High-valence calcium and magnesium ions act as charged salt ions that shield the electrostatic repulsion between SYGT molecules, causing the macromolecular chain to curl. The dehydration of inorganic salt ions removes the hydration water from the copolymer chain, reducing its hydrodynamic volume.

The lowest viscosity values (110.1 mPa·s, 114.88 mPa·s, and 146.59 mPa·s) were obtained with calcium salt, magnesium salt, and sodium salt concentrations of 3200 mg/L,

respectively. The corresponding viscosity loss rates were 61.4%, 60.65%, and 51.63%. These results indicate that the SYGT solution maintains a high viscosity even under high inorganic salt concentrations, with a relatively low viscosity loss rate.

2.6. Kinetics of Reaction

Using a rotating disk reaction system in a dynamic environment, the kinetic equations of the acid–rock reaction at various temperatures (120–180 °C) and acid concentrations (2.7–6 mol/L) were determined. The speeds of acid–rock reactions at various temperatures were contrasted. As an illustration, the data fitting of reaction kinetic parameters at 150 °C was used in Figure 11a. The J in the figure refers to the diffusion rate, which is the number of moles of material flowing through unit rock area per unit of time. The fitting effect was fair, and the fitting precision was 0.9599.

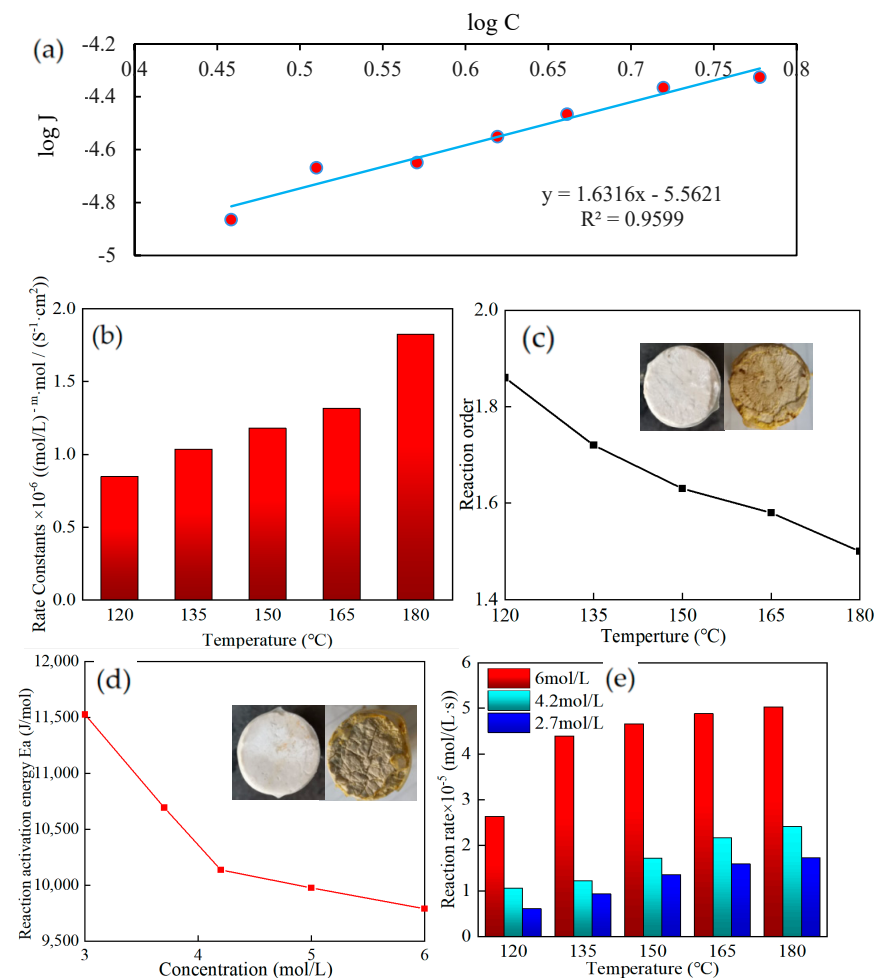


**Figure 11.** (a) Reaction kinetics parameter simulation at 150 °C; (b) Rate constant; (c) Reaction order; (d) Reaction activation energy; (e) Reaction rate.

The rate constant of the thickened acid solution added with SYGT and carbonate rock increased with increasing temperature, as shown in Figure 11b. The reaction order decreases with the increase in temperature, as shown in Figure 11c. Compared with 1.15 reaction order of VES at 120 °C [45], the reaction order of SYGT was 1.8 at 120 °C from the reaction results. At 180 °C, the acid–rock reaction order was 1.5, the rate constant was 1.82, and the reaction rate of 6 mol/L was  $5.03 \times 10^{-5}$  mol/(L·s). The thickening acid effectively controlled the reaction.

According to the physical meaning of the reaction order, the larger the reaction order, the greater the effect of concentration on the reaction rate [46]. The reaction order of the

thickened acid added to SYGT is higher than that of VES, which indicates that the acid concentration has a more obvious influence on it. The concentration of the acid solution increases the collision probability of the activated molecules. The more dependent it is on the concentration, the better its effect in slowing down the reaction.

The Arrhenius formula was used to determine the acid–rock reaction activation energy, as illustrated in Figure 11d. The graphic shows that as the acid concentration increases, the activation energy of the acid–rock interaction falls. The normal theory states that the activation energy of a reaction is a physical property that is independent of the concentration of the reactants. The acid–rock reaction, however, is an exothermic reaction, meaning that as it proceeds, a significant quantity of heat is generated, warming the surrounding area and increasing the acid–rock reaction. The acid concentration and the temperature cause the reaction to proceed in a positive-feedback way. The reaction speed is accelerated, as shown in Figure 11e.

### 2.7. Filtration of SYGT

Experiments were carried out to study the effect of static fluid loss on the thickening of acid over a temperature range of 120–180 °C. Linear regression analysis was performed on the experimental data to obtain the slope of the curve, and the parameters  $C_3$  and  $v_c$  in Equations (6) and (7) were calculated under different temperature conditions. The core before and after the experiment is shown in Figure 12. The core after the experiment clearly demonstrates the dissolution fractures that have undergone filtration and the acid solution that is being filtered. At 180 °C, the filtration coefficient and filtration velocity of the thickened acid were  $0.1747 \times 10^{-4}$  m/min<sup>0.5</sup> and  $0.2912 \times 10^{-5}$  m/min, respectively. It can be seen from the calculation results in Table 1 that the filtration loss of the acid solution under high-temperature conditions is well controlled.

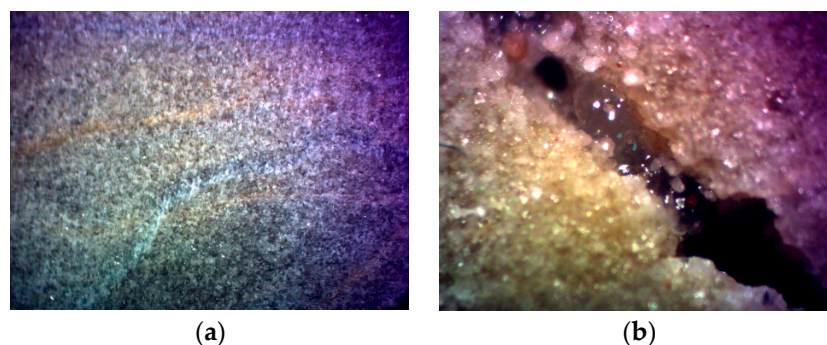


**Figure 12.** (a) Core before experiment; (b) Acid in the core and fractures after the experiment.

**Table 1.** Filtration coefficient and filtration rate.

Temperature	120 °C	135 °C	150 °C	165 °C	180 °C
Filtration coefficient $\times 10^{-4}$ (m/min <sup>0.5</sup> )	0.1031	0.1187	0.145	0.165	0.1747
Filtration rate $\times 10^{-5}$ (m/min)	0.1718	0.1978	0.2417	0.275	0.2912

### 2.8. Evaluation of the Conductivity of Acid-Etched Fractures

An acidizing fracturing conductivity tester was used to measure the acidizing fracturing conductivity of the natural core samples of Tadong Oilfield after being dissolved for 20 min using the thickened acid (10 mL/min injection rate, 180 °C ambient temperature). The measured results were compared with those of the field thickener after acidizing fracturing. The experimental results are shown in Figure 13.

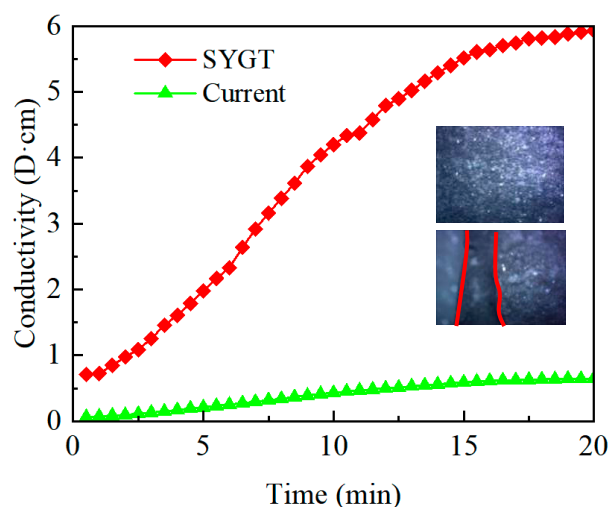


**Figure 13.** Conductivity of the thickened acid-etched fractures.

It can be seen from Figure 13 that after the SYGT-thickened acid dissolution, there are obvious acid-etched wormholes. In addition, the fracture conductivity of the SYGT-type thickened acid after dissolution is significantly higher than that of the on-site thickened acid, with the highest conductivity reaching 6 D·cm. The etching effect is significant after acid fracturing.

### 3. Material and Methods

#### 3.1. Materials

AM, AMPS, and NVP were sourced from Shanghai McLean Biochemical Technology Co., Ltd. (Shanghai, China). SSS was purchased from Beijing Datian Fengtuo Co., Ltd. (Beijing, China). Analytically pure reagents including NaOH, NaCl, CaCl<sub>2</sub>, and MgCl<sub>2</sub> were provided by Tianjin Yongda Chemical Reagent Factory, Tianjin, China. Deionized water was self-made in the laboratory. All chemicals and reagents were used without further purification.

#### 3.2. Synthesis of SYGT

In order to solve the problem of acid thickener failure under high-temperature conditions, AM, AMPS, NVP and SSS were used for polymerization in a water bath. The monomer ratio was designed to be 4AM:1AMPS:0.3NVP:0.3SSS for quaternary polymerization and 4AM:1AMPS:0.3SSS for ternary polymerization.

AM, AMPS, and NVP were mixed in deionized water, and NaOH solution was used to adjust the pH to 6 after stirring evenly. The temperature of the water bath was set at 40 °C. The rate of the agitator was adjusted to 300–350 r/min, and nitrogen was used to remove oxygen. After that, the temperature was set at 60 °C. During the heating process, K<sub>2</sub>S<sub>2</sub>O<sub>8</sub> was added to the three-neck flask. After the temperature reached 60 °C, the rotating rate was set at 150 r/min. After 2 h, a certain amount of SSS monomer was added to the flask and reacted for 12 h. Finally, the solution was purified in ethanol and dried in a vacuum for 12 h in an oven at 50 °C.

#### 3.3. Polymer Performance Evaluation

##### 3.3.1. Determination of Viscosity Average Molecular Weight

- (1) A total of 15 mL of the prepared 1000 mg/L polymer solution should be drawn with a pipette; it should be injected from viscometer tube A in Figure 14, and the temperature should be kept at 30.05 °C for 5 min.

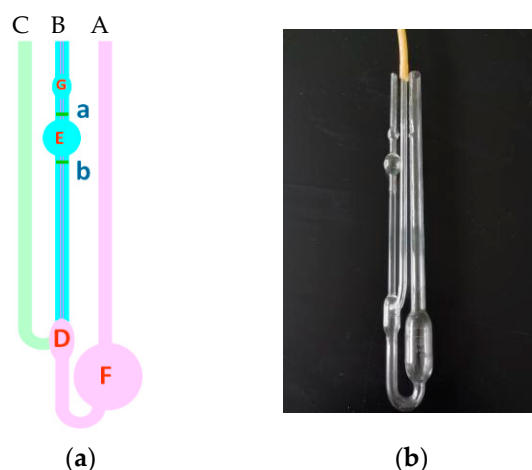


Figure 14. Schematic diagram of the Ubbelohde viscometer.

- (2) After constant temperature for 5 min, tube C should be pressed by hand, the ear ball should be placed at the mouth of tube B, the solution should be drawn into ball G, and it should be released.
- (3) When the solution drops to line a, the time should be recorded by pressing the stopwatch, and when the solution drops to line b, the experiment should be ended by pressing the stopwatch.
- (4) The measurement should be repeated three times, and the time difference between each time should not exceed 0.2 s.
- (5) After measuring the polymer solution with a concentration of 1000 mg/L, 1 mol/L NaCl solution should be sucked into the volumetric flask in a constant temperature bath using a pipette, and it should be added from tube a. Tube C should be pressed and held, and the solution should be repeatedly pressed and sucked from the orifice of tube B using a suction ear ball to make the mixture uniform.
- (6) The determination method is shown in (3) and (4).
- (7) Some 2 mL, 2 mL, and 4 mL of 1 mol/L NaCl solution should be added successively, and measured according to steps (5) and (6).
- (8) The relative viscosity of the sample solution should be calculated according to Formula (1):

$$\eta_r = \frac{t}{t_0} \quad (1)$$

where:  $\eta_r$ —relative viscosity;

$t$ —flow time of sample solution, s;

$t_0$ —flow time of 1 mol/L sodium chloride solution, s.

The corresponding  $[\eta_r] \cdot C$  value can be found from the obtained  $\eta_r$ , and the  $[\eta_r] \cdot C$  value can be divided by the sample concentration  $C$  to obtain  $[\eta_r]$ .

- (9) The molecular weight is calculated according to Formula (2):

$$[\eta] = KM^\alpha \quad (2)$$

where:  $M$ —average value of relative molecular weight of polymer;

$K$ —proportional constant,  $K = 3.34 \times 10^{-4}$ ;

$\alpha$ —empirical parameters related to the morphology of polymers in solution,  $\alpha = 0.708$ .

### 3.3.2. Thermogravimetric Analysis (TGA)

To investigate the thermal stability of SYGT, TGA experiments were conducted using STA449 F5 Jupiter, which is manufactured by NETZSCH in Selb, Germany). Nitrogen was used as both the purge gas and the protection gas at a flow rate of 60 mL/min. The temperature of SYGT was increased at a rate of 10 °C/min, ranging from 25 °C to 350 °C.

### 3.3.3. Infrared Spectrum Scanning

To confirm the successful synthesis of polymer SYGT, infrared scanning experiments were conducted using a Spectrum One FT-IR Spectrometer.

After the KBr powder was dried, 1 spoonful of SYGT solid was mixed with 3 spoonfuls KBr powder, and the two were uniformly mixed by grinding in a mortar. Finally the powder was pressed with a punch and scanned with the Spectrum One FT-IR Spectrometer.

### 3.3.4. Rheological Testing and Viscosity Testing of SYGT Aqueous Solution

The current thickener is ineffective when the viscosity keeps increasing at high temperatures. To investigate the physical mechanism of the phenomenon, the viscosity of its aqueous solution was measured using a HAAKE RheoStress 6000 (Thermo Fisher: Waltham, MA, USA) rotating rheometer at high temperatures (120–180 °C) under varying conditions, such as different shearing times and properties. The viscosity-increasing effects of both the SYGT and ternary polymers (AM/AMPS/SSS) were compared at high temperatures.

### 3.3.5. Reaction Kinetics of SYGT

The acid–rock reaction was conducted in a rotating disk system at temperatures ranging from 120 °C to 180 °C to determine the kinetics and activation energy of the reaction. This experiment aimed to investigate the reaction rate of the acid and rock with the synthetic thickener, and to explore the retarding effect of SYGT.

Data processing method:

In the processing of the actual test data, the reaction speed after correction of the face volume ratio is adopted:

$$J = -\left(\frac{\partial C}{\partial t}\right) \frac{V}{S} \quad (3)$$

Its principle formula is as follows:

$$J = kC^m \quad (4)$$

The  $C$  value and  $J$  value of Equation (2) can be measured under a certain temperature, pressure, and rotating speed using a rotating disc device. The acid rock reaction rate is determined using a differential method, and the relation curve is drawn:

$$J = \left(\frac{C_2 - C_1}{\Delta t}\right) \frac{V}{S} \quad (5)$$

For Formula (3), we obtained the following:

$$\lg J = \lg k + m \lg C \quad (6)$$

The reaction rate constant  $k$  and the reaction rate order  $m$  are constants under certain conditions. Therefore, a straight line is drawn using  $\lg J$  and  $\lg C$ , and the linear regression of  $\lg J$  and  $\lg C$  is carried out using the least-squares method to obtain the values of  $k$  and  $m$ , so as to determine the acid–rock reaction kinetic equation.

### 3.3.6. Static Fluid-Loss Test

At 120 °C, 150 °C, and 180 °C, static filter loss tests were performed, respectively, using six-link water loss equipment.

The filter loss factor is governed by the filter cake ( $C_3$ ), and the filter rate ( $v_c$ ) can be determined after sketching the static filtration curve of the fracturing fluid using Equations (7) and (8).

$$C_3 = 0.005 \times \frac{m}{A} \quad (7)$$

$$v_c = \frac{C_3}{\sqrt{t}} \quad (8)$$

where:  $C_3$ —filter loss factor controlled by filter cake,  $m/\sqrt{\text{min}}$ ;  
 $m$ —the slope of the filter loss curve,  $mL/\sqrt{\text{min}}$ ;  
 $A$ —the filtration area,  $\text{cm}^2$ ;  
 $v_c$ —the filter rate,  $\text{m}/\text{min}$ ;  
 $t$ —the filtration time,  $\text{min}$ .

#### 4. Conclusions

The synthesized SYGT is a cationic polyacrylamide with quaternary ammonium salt side chains. After conducting various experimental tests and analyzing the obtained results, the following conclusions may be drawn:

- (1) SEM and rheological analysis indicate that SYGT has good temperature and shear resistance. At 180 °C ( $100 \text{ s}^{-1}$ ), the viscosity of the SYGT aqueous solution is 316.52 mPa·s. Even after 160 min of shear, it still maintains a viscosity of 145.95 mPa·s. The thermogravimetric analysis shows that SYGT can withstand high temperatures up to 300 °C.
- (2) At 180 °C, the SYGT aqueous solution still has a minimum viscosity of 61.7 mPa·s at a 20%  $\text{H}^+$  concentration or high salt concentration. The reaction kinetics test proves that the SYGT-thickened acid effectively controls the reaction.
- (3) It was found that the polymer spatial network parameters have a substantial influence on the viscosity of polymer solutions. For the first time, the length and surrounding area of the SNS skeleton have been quantified. Our research demonstrates that there is a synergistic effect of the length and surrounding area on viscosity.

The synthesized SYGT has good temperature resistance, acid resistance, salt resistance, and shear resistance. SYGT can effectively fill the gap in the high-temperature field of carbonate-rock-thickening and acid-fracturing technology. In our future work, we will further explore the influence of SNS on the viscosity of polymer solutions.

**Author Contributions:** Y.S.: conceptualization; methodology; writing—original draft; writing—review and editing; investigation. T.G.: validation; data Curation; investigation; formal analysis. D.L.: supervision; formal analysis. D.G.: investigation. Z.Z.: methodology; resources. G.C.: methodology; funding acquisition; resources. All authors have read and agreed to the published version of the manuscript.

**Funding:** This research was funded by the National Natural Science Foundation of China, grant number 51574089.

**Institutional Review Board Statement:** Not applicable.

**Informed Consent Statement:** Not applicable.

**Data Availability Statement:** Not applicable.

**Acknowledgments:** Sui Yu and Guo Tianyue are supported by the China Scholarship Council. We thank the China Scholarship Council for their assistance.

**Conflicts of Interest:** The authors declare no conflict of interest.

#### References

1. Wei, W.; Varavei, A.; Sanaei, A.; Sepehrnoori, K. Geochemical modeling of Wormhole propagation in carbonate acidizing considering Mineralogy heterogeneity. *SPE J.* **2019**, *24*, 2163–2181. [[CrossRef](#)]
2. Yan, T.; Xu, R.; Sun, S.-H.; Hou, Z.-K.; Feng, J.-Y. A real-time intelligent lithology identification method based on a dynamic felling strategy weighted random forest algorithm. *Pet. Sci.* **2023**. [[CrossRef](#)]
3. Schwalbert, P.; Aljawad, M.; Saleh, M.; Hill, D.A.; Zhu, D. Decision Criterion for Acid-Stimulation Method in Carbonate Reservoirs: Matrix Acidizing or Acid Fracturing? *SPE J.* **2020**, *25*, 2296–2318. [[CrossRef](#)]

4. Lv, Y.; Wei, P.; Zhu, X.; Gan, Q.; Li, H. THMCD modeling of carbonate acidizing with HCl acid. *J. Pet. Sci. Eng.* **2021**, *206*, 108940. [[CrossRef](#)]
5. Du, J.; Guo, G.; Liu, P.; Xiong, G.; Chen, P.; Liu, J.; Chen, X. Experimental Study on the Autogenic Acid Fluid System of a High-Temperature Carbonate Reservoir by Acid Fracturing. *ACS Omega* **2022**, *7*, 12066–12075. [[CrossRef](#)] [[PubMed](#)]
6. Lu, N.; Dong, X.; Chen, Z.; Liu, H.; Zheng, W.; Zhang, B. Effect of solvent on the adsorption behavior of asphaltene on silica surface: A molecular dynamic simulation study. *J. Pet. Sci. Eng.* **2022**, *212*, 110212. [[CrossRef](#)]
7. Dang, L.; Zhou, C.; Huang, M.; Jiang, D. Simulation of effective fracture length of prepad acid fracturing considering multiple leak-off effect. *Nat. Gas Ind. B* **2019**, *6*, 64–70. [[CrossRef](#)]
8. Liang, X.; Zhou, F.; Liang, T.; Huang, Y.; Wei, D.; Ma, S. The effect of combined proppants upon the fracture conductivity in tight gas reservoirs. *Energy Rep.* **2020**, *6*, 879–884. [[CrossRef](#)]
9. Chen, C.; Wang, S.; Lu, C.; Liu, Y.; Guo, J.; Lai, J.; Tao, L.; Wu, K.; Wen, D. Experimental study on the effectiveness of using 3D scanning and 3D engraving technology to accurately assess shale fracture conductivity. *J. Pet. Sci. Eng.* **2022**, *208 Part C*, 109493. [[CrossRef](#)]
10. Mehrjoo, H.; Norouzi-Apourvari, S.; Jalalifar, H.; Shajari, M. Experimental study and modeling of final fracture conductivity during acid fracturing. *J. Pet. Sci. Eng.* **2022**, *208 Part B*, 109192. [[CrossRef](#)]
11. Wang, X.; Wang, L.; Liu, K.; Zhu, C.; Guan, F. Study on degradation of wastewater containing PAM catalyzed by nonequilibrium plasma and  $\gamma$ -Al<sub>2</sub>O<sub>3</sub>. *J. Water Process Eng.* **2022**, *49*, 103065. [[CrossRef](#)]
12. Xu, Z.; Qi, N.; Zhang, Z.; Han, Z.; Su, X. Development and evaluation of authigenic acid system in high-temperature carbonate reservoirs. *IOP Conf. Ser. Earth Environ. Sci.* **2021**, *781*, 022015. [[CrossRef](#)]
13. Liu, K.; Cao, J.; Jiao, K.; Li, Y. Research progress of slow-release acid system. *Spec. Petrochem.* **2022**, *39*, 68–73.
14. Guo, Y.; Sun, Y.; Shen, K.; Ran, H. Research and exploration on acidizing fracturing technology in oilfield. *IOP Conf. Ser. Earth Environ. Sci.* **2021**, *859*, 012065. [[CrossRef](#)]
15. Li, P.; Lai, X.; Wang, L.; Li, P.; Gao, J.; Zhang, X.; Liu, G. Synthesis and properties of high-temperature resistant acid thickener. *Fine Chem.* **2022**, *39*, 411–416+432.
16. Yu, Y.; Cui, J.; Zhang, R.; Yin, H.; Feng, Y. Gelling Acid Thickener for Oil and Gas Production: Preparation, Properties and Applications. *Oilfield Chem.* **2021**, *38*, 553–559.
17. Liu, J.; Almakimi, A.; Wei, M.; Bai, B.; Hussein, I.A. A comprehensive review of experimental evaluation methods and results of polymer micro/nanogels for enhanced oil recovery and reduced water production. *Fuel* **2022**, *324 Part B*, 124664. [[CrossRef](#)]
18. Du, J.; Liu, J.; Zhao, L.; Liu, P.; Chen, X.; Wang, Q.; Yu, M. Water-soluble polymers for high-temperature resistant hydraulic fracturing: A review. *J. Nat. Gas Sci. Eng.* **2022**, *104*, 104673. [[CrossRef](#)]
19. Luo, Y.; Fang, B.; Lu, Y.; Qiu, X.; Guan, B.; Li, K. Research Progress of High Temperature Fracturing Fluid. *Oilfield Chem.* **2018**, *35*, 545–549.
20. Jiang, Q.; Yang, X.; Gong, F. Development and evaluation of high temperature resistant cross-linked acid fracturing fluid system. *Chem. Ind. Eng.* **2022**, *39*, 51–57.
21. Yang, Y.; Fenjuan, G.; Li, L.; Chao, Y.; Wei, Q.; Fei, L.; Wang, X. Optimization and application of self-association fracturing fluid. *Fault-Block Oil Gas Field* **2021**, *28*, 566–570.
22. Gan, J.; Wang, D.; Xiao, Z.; Li, S.; Zhang, K.; Zhu, X. Synthesis and performance of a novel high-efficiency coal dust suppressant based on biopolysaccharide xanthan gum. *Fuel* **2022**, *329*, 125442. [[CrossRef](#)]
23. Gao, M.; Jiang, J. Preparation and properties of a water-based fracturing fluid system. *Petrochem. Technol.* **2020**, *49*, 1188–1193.
24. Zhao, Z.; Liu, T.; Luo, P.; Li, Y.; Liu, J.; Cheng, J.; Yu, Y. Performance and field implementation of a new fracturing fluid consisting of hydrophobically associating polyacrylamide and anionic surfactant. *J. Polym. Eng.* **2016**, *36*, 13–21. [[CrossRef](#)]
25. Sui, Y.; Cao, G.; Guo, T.; Li, Z.; Bai, Y.; Li, D.; Zhang, Z. Development of gelled acid system in high-temperature carbonate reservoirs. *J. Pet. Sci. Eng.* **2022**, *216*, 110836. [[CrossRef](#)]
26. Tian, Y.; Zhang, S.; Song, A. Development and Evaluation of a Salt-Tolerant Instant Seawater-Based Fracturing Fluid System. *J. Jiangnan Univ. Nat. Sci. Ed.* **2021**, *49*, 65–72.
27. Ma, X.; Sun, X.; Chang, M.; Liu, Q.; Dong, X.; Fan, Y.; Chen, R. Adsorption of Different Ionic Types of Polyacrylamide on Montmorillonite Surface: Insight from QCM-D and Molecular Dynamic Simulation. *Molecules* **2023**, *28*, 4417. [[CrossRef](#)]
28. Hue, K.Y.; Lew, J.H.; Myo Thant, M.M.; Matar, O.K.; Luckham, P.F.; Müller, E.A. Molecular Dynamics Simulation of Polyacrylamide Adsorption on Calcite. *Molecules* **2023**, *28*, 6367. [[CrossRef](#)]
29. Tarasova, N.; Zanin, A.; Krivoborodov, E.; Toropygin, I.; Pascal, E.; Mezhev, Y. The New Approach to the Preparation of Polyacrylamide-Based Hydrogels: Initiation of Polymerization of Acrylamide with 1,3-Dimethylimidazolium (Phosphonoxy-)Oligosulphanide under Drying Aqueous Solutions. *Polymers* **2021**, *13*, 1806. [[CrossRef](#)]
30. Gbadamosi, A.; Patil, S.; Kamal, M.S.; Adewunmi, A.A.; Yusuff, A.S.; Agi, A.; Oseh, J. Application of Polymers for Chemical Enhanced Oil Recovery: A Review. *Polymers* **2022**, *14*, 1433. [[CrossRef](#)]
31. Simeonov, M.; Apostolov, A.A.; Georgieva, M.; Tzankov, D.; Vassileva, E. Poly(acrylic acid-co-acrylamide)/Polyacrylamide pIPNs/Magnetite Composite Hydrogels: Synthesis and Characterization. *Gels* **2023**, *9*, 365. [[CrossRef](#)]
32. Ding, F.; Dai, C.; Sun, Y.; Zhao, G.; You, Q.; Liu, Y. Gelling Behavior of PAM/Phenolic Crosslinked Gel and Its Profile Control in a Low-Temperature and High-Salinity Reservoir. *Gels* **2022**, *8*, 433. [[CrossRef](#)]

33. Song, H.; Zhang, S.-F.; Ma, X.-C.; Wang, D.-Z.; Yang, J.-Z. Synthesis and application of starch-graft-poly(AM-Co-AMPS) by using a complex initiation system of CS-APS. *Carbohydr. Polym.* **2007**, *69*, 189–195. [[CrossRef](#)]
34. Xu, J.; Wu, Y.M.; Wang, C.X.; Wang, Y.P. Dispersion polymerization of acrylamide with 2-acrylamide-2-methyl-1-ropane sulfonate in aqueous solution of sodium sulfate. *J. Polym. Res.* **2009**, *16*, 569–575. [[CrossRef](#)]
35. Liao, Y.; Zheng, H.; Qian, L.; Sun, Y.; Dai, L.; Xue, W. UV-Initiated polymerization of hydrophobically associating cationic polyacrylamide modified by a surface-active monomer: A comparative study of synthesis, characterization, and sludge dewatering performance. *Ind. Eng. Chem. Res.* **2014**, *53*, 11193–11203. [[CrossRef](#)]
36. Zhong, C.R.; Zhang, H.; Feng, L.M. Solution behavior and associating structures of a salt-tolerant tetra-polymer containing an allyl-capped macromonomer. *JP Olym. Res.* **2014**, *21*, 1–9. [[CrossRef](#)]
37. Cao, J.; Liu, K.; Xu, G.; Liu, C.; Zhen, W.; Wang, J. Preparation and properties of a double quaternary ammonium copolymer used in acid fracturing. *Petroleum* **2022**, *9*, 265–273. [[CrossRef](#)]
38. Levitt, D.; Pope, G.A. Selection and Screening of Polymers for Enhanced-Oil Recovery, Society of Petroleum Engineers. In Proceedings of the SPE Symposium on Improved Oil Recovery, Tulsa, OK, USA, 20–23 April 2008. [[CrossRef](#)]
39. Ma, X.; Mu, H.; Hu, Y.; Yang, S. Synthesis and properties of hydrophobically associating polymer fracturing fluid. *Colloids Surf. A Physicochem. Eng. Asp.* **2021**, *626*, 127013. [[CrossRef](#)]
40. Zana, R. Dimeric and oligomeric surfactants. Behavior at interfaces and in aqueous solution: A review. *Adv. Colloid Interface Sci.* **2002**, *97*, 205–253. [[CrossRef](#)] [[PubMed](#)]
41. Zhang, Y.; Mao, J.; Zhao, J.; Yang, X.; Zhang, Z.; Yang, B.; Zhang, W.; Zhang, H. Preparation of a novel ultra-high temperature low-damage fracturing fluid system using dynamic crosslinking strategy. *Chem. Eng. J.* **2018**, *354*, 913–921. [[CrossRef](#)]
42. Lu, H.; Liu, Y.; Wang, B.; Zheng, C.; Huang, Z. Self-assembling transition behavior of a hydrophobic associative polymer based on counterion and pH effects. *Colloids Surf. A Physicochem. Eng. Asp.* **2016**, *490*, 1–8. [[CrossRef](#)]
43. Zhang, X.; Han, M.; Xu, L.; AlSofi, A.M. Long-term stability prediction of polyacrylamide-type polymers at harsh conditions via thermogravimetric analysis. *Chem. Phys. Lett.* **2022**, *795*, 139538. [[CrossRef](#)]
44. Xu, X.; Xiong, G.; Chen, G.; Fu, T.; Yu, H.; Wu, J.; Liu, W.; Su, Q.; Wang, Y.; Liu, S.; et al. Characteristics of coastal aquifer contamination by seawater intrusion and anthropogenic activities in the coastal areas of the Bohai Sea, eastern China. *J. Asian Earth Sci.* **2021**, *217*, 104830. [[CrossRef](#)]
45. Zhong, X.; Zhang, R.; Wu, G.; Yin, Z.; Wang, X.; Lu, H.; Gao, Y. Study on Dynamic Characteristics of Acid Rock Reaction and Acid Fracturing Countermeasures in Complex Heterogeneous Carbonate. *Drill. Fluid Complet. Fluid* **2020**, *37*, 798–802. [[CrossRef](#)]
46. Sui, Y.; Cao, G.; Guo, T.; Zhang, Z.; Bai, Y.; Wu, J.; Yao, L. Evaluation of deep penetration of high-temperature sustained-release acid based on the reaction kinetics and conductivity of acid-etched fractures. *Case Stud. Therm. Eng.* **2022**, *38*, 102336. [[CrossRef](#)]

**Disclaimer/Publisher’s Note:** The statements, opinions and data contained in all publications are solely those of the individual author(s) and contributor(s) and not of MDPI and/or the editor(s). MDPI and/or the editor(s) disclaim responsibility for any injury to people or property resulting from any ideas, methods, instructions or products referred to in the content.